Chapter 4

Remote Sensing in Land Applications by Using GNSS-Reflectometry

Yan Jia and Yuekun Pei

Additional information is available at the end of the chapter

http://dx.doi.org/10.5772/intechopen.72901

Abstract

Global navigation satellite system-reflectometry (GNSS-R) as an efficient tool for remote sensing has gained increasing interests in the last two decades, due to its unique characteristics. It uses GNSS signals as sources of opportunity, providing precise, continuous, all-weather, and 24 hours' detections, which play a key role in many land applications. The fundamental theoretical part of GNSS-R technique is examined at first. Then, GNSS-R methodologies applied in the soil moisture content, vegetation biomass sensing, and altimetry applications are also detailed. One retrieval method uses only RH (right-hand) reflected data. Another retrieval method for soil moisture content (SMC) aimed to calibrate the measurement by using water reflections, based on the bistatic equations with LH (left-hand) reflected and RH direct signals. The other method for SMC retrieval is related to the polarimetric ratio (PR), the ratio of LH/RH reflected signals can reveal the fluctuations of the SMC. Another vital parameter vegetation biomass was observed by using the variation of reflectivity of the LH and RH reflected components. Finally, the C/A code method was used for exploring the possibility to the altimetry estimation. The features of GNSS-R technique made it a promising remote sensing technique in hydrology, climatology carbon cycles, and other potential applications.

Keywords: GNSS-reflectometry (GNSS-R), soil moisture content, vegetation biomass, altimetry, polarimetric measurement

1. Introduction to GNSS

Global navigation satellite systems (GNSSs) are satellite constellations orbiting the Earth to provide continuous positioning and timing information for users on the globe. It mainly includes the United States' NAVSTAR global positioning system (GPS), European Union's Galileo, Russia's Glonass, China's BeiDou, and Japan's Quasi-Zenith satellite system (QZSS). For now,

such systems are used not only for navigation positioning but also for object detection in various disciplines, such as archeology (a 3-dimension map is generated using the combined signals of GPS, Glonass, and QZSS to detect each artifact), air traffic (the surveillance-broadcast system of air traffic control obtains aircraft positions by using GNSS signals), weather (forecast can be made through the atmospheric bending measurement of GNSS satellite signals), and others. The huge potential of GNSSs has led international governments and researchers made efforts on it [1]. Up to now, the United States' NAVSTAR GPS and the Russian GLONASS have begun providing global coverage for a long time. In December 2016, the European's Galileo formally announced to start its initial service to provide its full operational capability. China is in the process of expanding its regional BeiDou Navigation Satellite System into global compass navigation system in the very near 2020. India and Japan are also in the process of developing their regional navigation systems [2].

1.1. GPS system

GPS is the United States' global positioning system (GPS) developed since 1973. The number of satellites, the positions, and the relative inclinations was optimized to ensure an adequate global coverage. In 1978, the first operational prototype satellite was launched. In 1993, the initial capability and the full GPS system were declared [3]. As a universal positioning system, GPS provides an accurate, continuous, three-dimensional position and velocity information to the user with the appropriate receiver on Earth. Now, it is the most used navigation system in the world and fully operative both for military purpose and civilian aims [4].

The GPS signals are transmitted with right-hand circular polarization (RHCP) so that the ionosphere attenuation does not affect the signal reception. Each GPS satellite transmits

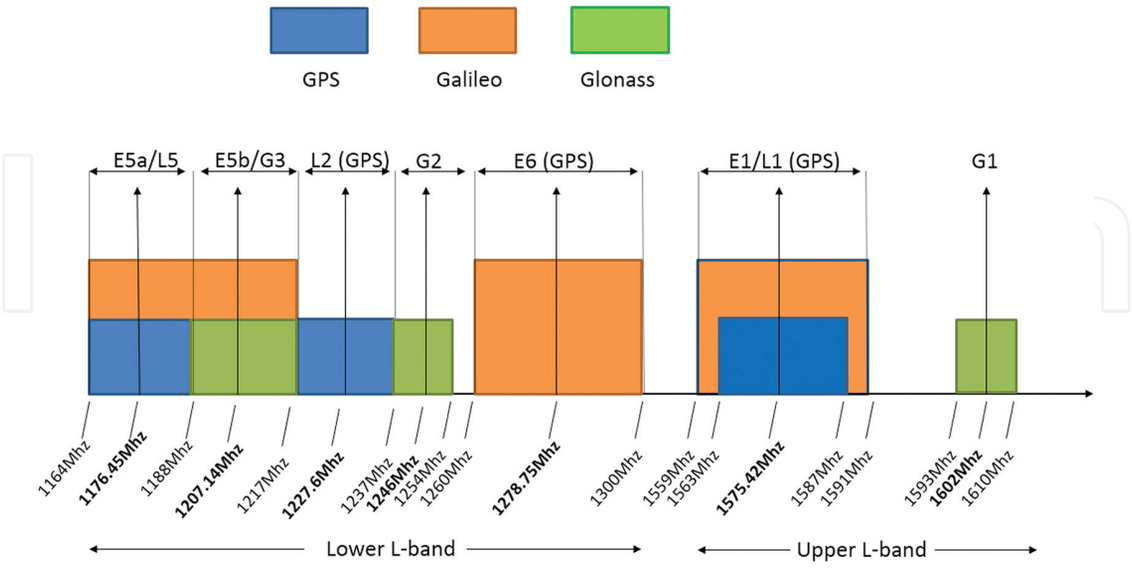

Figure 1. GNSS frequency bands.

microwave carrier signals at three bands: L1 (1575.42 MHz) carries the navigation message and the standard positioning services (SPS), L2 (1227.6 MHz) is used to measure the ionosphere delay by precise positioning services (PPS), and L5 (1176.45 MHz) was introduced to increase the accuracy for safety-of-life transportation applications [5]. The frequency plan and the band of GPS are shown in **Figure 1**, together with the information of Galileo and Glonass [6].

2. Theory of GNSS-reflectometry

GNSS-reflectometry is usually called for short as GNSS-R. Its main principle is to receive and further extract information from the GNSS signals which were reflected off the Earth surface. It works as a bistatic radar, in which the transmitter and the receiver are separated by a significant distance, comparable to the expected distance to the target. The concept can be expanded that the receiver receives multiple signals simultaneously from different transmitters, in which case, it is multistatic radar. Comparing with the other existing remote sensing tools, GNSS-R has following advantages: 1. The additional transmitter is not needed; 2. Many signal sources can be chosen, including GPS, Galileo, GLONASS, and BeiDou/Compass; 3. Use spread-spectrum communication technology for receivers to receive weak signals; 4. It provides a wide range of applications, for example, soil moisture retrieval, vegetation biomass detection, altimetry estimation, sea wind and wave height, and so on [1, 7–13].

2.1. GNSS-R geometry

In the case of GNSS-reflectometry, the transmitter and receiver are in the different locations, and the scattered signals can be originated from a variety of geometries, given a target that scatters sufficient power to the direction of the receiver. For the land surface, the typical bistatic geometry consists of a transmitter and receiver above the surface, with scattering taking place mainly from the region of the surface surrounding a specular reflection point. The specific geometry is depicted in **Figure 2**.

Figure 2 depicts signals transmitted from a GPS satellite (about 20,200 km height), scattered from the land surface along the specular direction, and received by a receiver equipped on an aircraft. The direct signal is received by the zenith antenna for processing positioning information or system calibration, and the reflected signal is received by the nadir antenna for remotely sensing the land surface. The incident RHCP GPS signal is predominantly left-hand circular polarization (LHCP) after specular scattering. The specular point is defined as a reflection point characterized that the incident and reflected angles are equal (Snell's Law). The strong coherent scattering component concentrated about a narrow area called the first Fresnel zone around the specular point. The size of this active region is usually considered to be the first Fresnel zone for which the differential phase change across the surface is constrained to $\lambda/2$ radians, where λ is the signal wavelength [14]. Surface roughness causes scattering from a

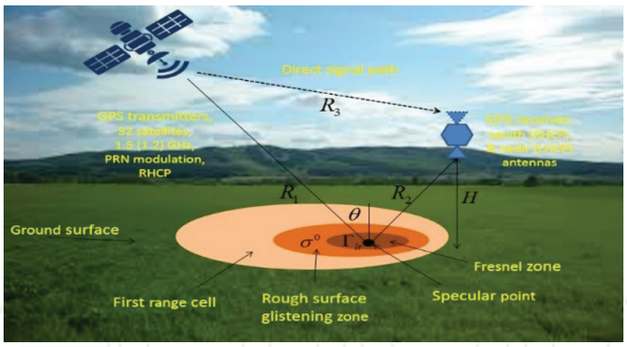

Figure 2. GNSS-R as a bistatic radar geometry.

glistening zone around the specular reflection point. The scattering component, also called incoherent or diffuse component, consists of power scattered randomly in all directions, with its magnitude smaller than coherent component.

When the distance from the surface to the transmitter is much larger than the distance from the surface to the receiver (or vice versa), the semi-major axis a and semi-minor axis b of the first Fresnel ellipse are dependent on the incidence angle θ, and minimum height of the transmitter or receiver H was given by [15]:

$$\alpha = \frac{\sqrt{2\delta H \cos(\vartheta)}}{(\cos(\theta))^2}, b = \frac{\sqrt{2\delta H \cos(\theta)}}{\cos(\theta)}, \tag{1}$$

where δ is the phase change measured in wavelengths ($\lambda/2$ for the first Fresnel zone) and θ is the incident angle.

As the signal scattering, the time delay and the frequency of the received signals change. The narrowly spaced iso-range ellipses (lines of equal delay across the surface) and iso-Doppler hyperbolas (lines of equal Doppler frequency across the surface) can be mapped across the Earth as shown in **Figure 3**. At each point in the glistening zone, the path delay and reflection angles are different. This results in a range of different path delays (between the transmitter and receiver) and Doppler frequencies at the receiver. Lines of constant delay or iso-range lines can be drawn as ellipses centered at the point of specular reflection. The lines with the same radial velocity are the cuts of the cone surfaces with the earth plane, i.e., parabola. At fixed radio frequency (RF), the radial velocity is proportional to the Doppler frequency. Therefore, the cone can also be called Doppler cone, and the cone cuts with the earth surface called iso-Doppler lines [16, 17].

In **Figure 3**, the red ellipses represent the first Fresnel zone. The uneven ring belts indicate equal-code delay lines (yellow lines). The black curves are the Equal-Doppler lines. GPS satellites are far from the Earth and thus the Fresnel belts are small. The surface property can be extracted through analyzing the reflected signal and the direct one.

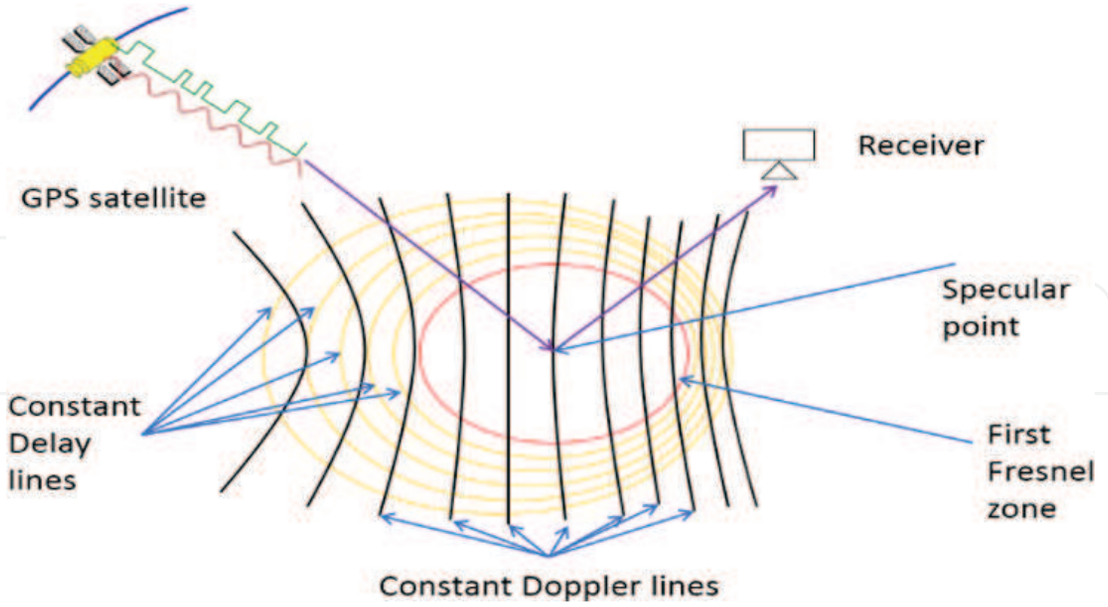

Figure 3. Iso range and iso-Doppler lines across the Earth's surface around the specular reflection point.

2.2. Bistatic radar equations

In general, the total scatter power p^r_{pq} measured by a bistatic radar can be expressed as [18]:

$$p^r_{pq} = p^c_{pq} + p^i_{pq}, \tag{2}$$

where subscripts q and p denote the incident and scattered polarizations. p^c_{pq} and p^i_{pq} are the coherent power and incoherent power, respectively.

2.2.1. Coherent component from smooth surface

For the coherent component in the case of like polarized GPS bistatic radar, the bistatic equation can be written as [18],

$$P^c_{lr} = \frac{P^t_r G^t}{4\pi(R_{st} + R_{rs})^2} \frac{G^r \lambda^2}{4\pi} \Gamma_{lr}. \tag{3}$$

Subscript lr represents the scattering when a satellite incident signal (right-hand polarized) is scattered by the surface and inverts the polarization to the left-hand, P^t_r is the transmitted RHCP signal power, G^t is the transmitter antenna gain, G^r is the receiver antenna gain, and λ is the wavelength (19.042 cm for GPS L1 signal). R_{rs} is the distance between the receiver and the specular point, R_{st} is the distance between the satellite and the specular point, and Γ_{lr} is the power reflectivity of the reflecting surface.

2.2.2. Coherent component from rough surface

As the smooth surface begins to transition to a rough surface, the coherent component of the reflected power is decreased. Therefore, the term Γ_{lr} in Eq. (3) decreased from that of the smooth surface case due to increasing roughness, which was described by [14].

$$\Gamma_{lr}(\theta) = |R_{lr}(\theta)|^2 \chi(z), \tag{4}$$

where R_{lr} is the Fresnel reflection coefficient and $\chi(z)$ is the probability density function of the surface height z.

The Fresnel reflection coefficient R_{lr} can be expressed as linearly polarization modes [7]:

$$R_{lr} = R_{rl=} \frac{1}{2}(R_{vv} - R_{hh}), \tag{5}$$

$$R_{rr} = R_{ll=} \frac{1}{2}(R_{vv} + R_{hh}), \tag{6}$$

where R_{vv} and R_{hh} are the Fresnel coefficients for horizontal and vertical polarization [19]:

$$R_{hh}(\theta) = \frac{\cos\theta - \sqrt{\varepsilon_r - \sin^2\theta}}{\cos\theta + \sqrt{\varepsilon_r - \sin^2\theta}}, \tag{7}$$

$$R_{vv}(\theta) = \frac{\varepsilon_r \cos\theta - \sqrt{\varepsilon_r - \sin^2\theta}}{\varepsilon_r \cos\theta + \sqrt{\varepsilon_r - \sin^2\theta}}, \tag{8}$$

$$\varepsilon_r = \varepsilon/\varepsilon_0 - j60\lambda\sigma, \tag{9}$$

where θ is the incident angle, in which ε is the dielectric constant of the surface, ε_0 is the dielectric constant of the air, λ is the wavelength of the signal, and σ is the electric conductivity.

Most of the natural surface can be modeled by a Gaussian height distribution. Thus, the reflectivity can be written as:

$$\Gamma_{lr}(\theta) = |R_{lr}(\theta)|^2 e^{-h(\cos\vartheta)^2}. \tag{10}$$

h was called roughness parameter, and it is defined as:

$$h = 4k^2\sigma^2, \tag{11}$$

where k is the wave number ($2\pi/\lambda$) and σ is the standard deviation of the surface. When it is a smooth surface ($h = 0$), the reflectivity R_{lr} is simply the square of the Fresnel reflection coefficient.

2.3. Coordinate reference systems

Latitude, longitude, and height are three coordinates used to characterize the user's position on Earth. A reference system with respect to the coordinates must be defined correspondingly.

In the beginning, the World Geodetic System 1984 ellipsoid (WGS84) in an Earth-centered, Earth-fixed (ECEF) coordinate system is defined for typical GPS measurements. The ECEF coordinates represent positions as (x, y, z). The x-axis points in the direction of 0° longitude (passing through the intersection of the Greenwich meridian with the equatorial plane), and the +y-axis points in the direction of 90° east longitude. The z-axis is chosen to be normal to the equatorial plane in the direction of the geographical north pole, thereby completing the right-handed coordinate system. The ECEF system enables users to know the positions with respect to the center of the Earth. The ellipsoid coordinate origin of WGS84 (latitude, longitude, and attitude) is meant to be located at the Earth's center of mass. It is a simplest geometric model, which best fits the entire Earth surface [20].

Since the Earth is not spherical and not uniform in density, the Earth Geoid Model 1996 (EGM96) was defined as the locus of all points with the same gravity potential (equipotential surface) best fitting with the mean sea level on the Earth [21]. When the height is indicated relevant to the mean sea level, it refers to the geoid model. The height of the geoid is denoted N with respect to the ellipsoid, which is shown in **Figure 4**. At each point, a geoidal height (N) is defined along the line perpendicular to the ellipsoid. It is measured from the ellipsoid to the geoid. Height h is the distance measured from the ellipsoid to the object. H indicates the height with respect to the geoid called orthometric height.

Georeferencing specular points on maps were done based on the ECEF coordinate system, by assuming the surface is locally flat and the surface height remains the same with that of the receiver projection position. However, a typical onboard GPS receiver and Google Earth software provide the ellipsoid height h based on the EGM96 model. Therefore, the EGM96 coordinates information was transferred in WGS84 and further converted to ECEF coordinates, in order to calculate the elevation angle with respect to the satellite position (x, y, z). On the other hand, the orthometric height H is useful, such as in the altimetry application. Hence, some computations are needed as Eq. 12 [3].

$$H \approx h - N. \tag{12}$$

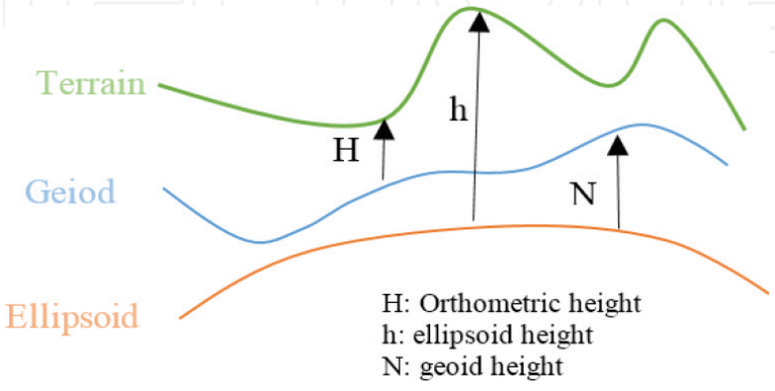

Figure 4. Relation of an ellipsoid, geoid, and terrain heights.

3. GNSS-R applications

3.1. Background and objective

After GNSS signals reflected off the Earth surface, the scattered signal received by the GNSS-R system contains the information of the surface. Hence, GNSS-R as an Earth's surface remote sensing tool has been widely studied for characterizing the reflecting surface. Several retrieval methods for soil moisture content (SMC), altimetry, and vegetation biomass estimation can be used to reveal the geographical and biological parameters of the Earth surface.

For altimetry application, the GPS Bistatic technique for altimetry application was first proposed by Martin-Neira [17]. The aim of the GNSS altimetry is to detect the height between the receiver and the reflecting surface. In principle, the altimetry techniques can be applied to any surface, but their performance will depend on the detecting environment [22–24].

For soil moisture application, frequencies in the range of 1–3 GHz have been shown to be ideally suited to sense soil moisture due to reduced atmospheric attenuation [25]. Njoku and O'Neill [26] showed that P-band (0.775 GHz) and L-band (1.4 GHz) frequencies are optimal for sensing soil moisture in the top 0–4 and 0–2 cm surface layers, respectively.

For biomass content sensing, a couple of papers mentioned that a retrieval method with very preliminary analysis is available. The one provided by Zavorotny et al. [27] proposed modeling GPS reflected signals having a different polarization state that can be used for sensing a homogeneous soil of rough land surface. The results were obtained by modeling the impact of soil moisture from the ratio between expected power levels in orthogonal polarizations (LR/RR, HR/VR), in function of the elevation angle. By varying the soil moisture level (x-axis) and different incident angles (the angle between the propagation path and the normal to the surface), the ratio of two orthogonal polarizations received power proved to be independent of the surface roughness factor and sensitive to the soil moisture. With this established theoretical hypothesis, the algorithm with respect to the orthogonal polarization was developed and presented as follows.

In the following, the retrieval methods for the SMC, vegetation sensing, and altimetry applications are applied and discussed in the framework of Italian SMAT-F2 (System of Advanced monitoring of the Territory—phase 2) project. First, the SMC retrieval and vegetation biomass sensing methods are detailed. With considering different kinds of measured signals, three kinds of retrieval methods based on the bistatic configuration are presented. Then, the C/A code altimetry method, which provides the possibility for altimetry estimation, will be discussed.

3.2. Methodologies

3.2.1. Overview of soil moisture retrieval methods

Soil dielectric constant and soil moisture retrieval play fundamental aspects in agriculture and water cycle attracting interests from many researchers and have started to produce some results. Three different methodologies were implemented mainly for this kind of applications:

1. Multipath effect and its relation to soil moisture: it uses a standard ground-based nearly hemispherical RHCP antenna to receive the direct signal (see **Figure 5(a)**). The reflected signal originated from ground creates multipath effects, since it interferes with the direct signal. The total received signal amplitude has a sinusoid behavior with the change of sine of elevation angle. By measuring the received SNR ratio, it is possible to retrieve soil moisture information [9, 27].
2. Interference pattern technique (IPT): usually a horizontal-pointing vertically polarized antenna is used (see **Figure 5(b)**). This technique consists of measuring the power fluctuations related to the signal resulting from the simultaneous reception (and interference) of the direct and the reflected GNSS signals. It is similar to a multipath effect. In this case, the two rays approach is adopted. Soil moisture retrieval is based on finding a specific 'notch' point from the interference pattern, versus satellite elevation [22, 28–30].
3. Bistatic method: this is based on the separate reception of direct and reflected signals using two different antennas and on the separate measurement of signal powers. Depending on the antenna configuration, three possible observing systems exploiting the bistatic geometry can be further identified:
    a. A down-looking LHCP antenna and an up-looking RHCP antenna: an LHCP antenna receives reflected GPS signal from the surface (see **Figure 5(c)**). The power reflectivity could be obtained either by using a bistatic radar equation [31] or from the power ratio between the reflected signal and the direct signal [32, 33]. The reflectivity is then a function of the dielectric constant of the soil, the elevation angle, and the surface roughness. By properly choosing the surface roughness parameter (elevation is known from the direct signal) for a certain scattering model (see for example [34]) such as the small perturbation method (SPM) and Kirchhoff approach (KA), the dielectric constant can be retrieved.
    b. One RHCP up-looking antenna and two down-looking antennas (or channels) with one RHCP polarized and the other LHCP polarized [7, 12, 35]. With this configuration (see **Figure 5(d)**), it is possible to measure both the co-polar component of the terrain reflectivity by using the LHCP signal and the cross-polar component by using the RHCP antenna. The ratio of these two reflectivities was in good correlation with SMC, and it was independent of the surface roughness.
    c. A similar configuration to the one described in (3.a) but with horizontally (H) and vertically (V) polarized antenna for both the up and down-looking directions (see **Figure 5(e)**): this configuration has been tested through some simulation studies [36]. The ratio between the reflected and the direct power on the horizontal polarization and the same ratio on the vertical polarization depend on the soil reflectivity and surface roughness. If the power ratio between the two channels with orthogonal polarization is considered, the influence of the surface roughness can be canceled. It was verified that the final expression holds under different scattering models, which means that it could be applied to a wide range of surface roughness. This dielectric constant retrieval approach is based on the use of the ratio of power densities scattered

at *HH* and *VV* polarizations along the specular direction for different incidence angles. Since the ratio is a function of both the elevation angle and the dielectric constant, a minimum least square technique was applied to better define the dielectric constant, by measuring at least two different elevation angles.

The retrieval of the soil moisture from the dielectric constant at microwave band (especially in L band) has been widely investigated, and several well-accepted theoretical and empirical models have been established, such as [25, 28, 37, 38]. The information of soil texture in terms

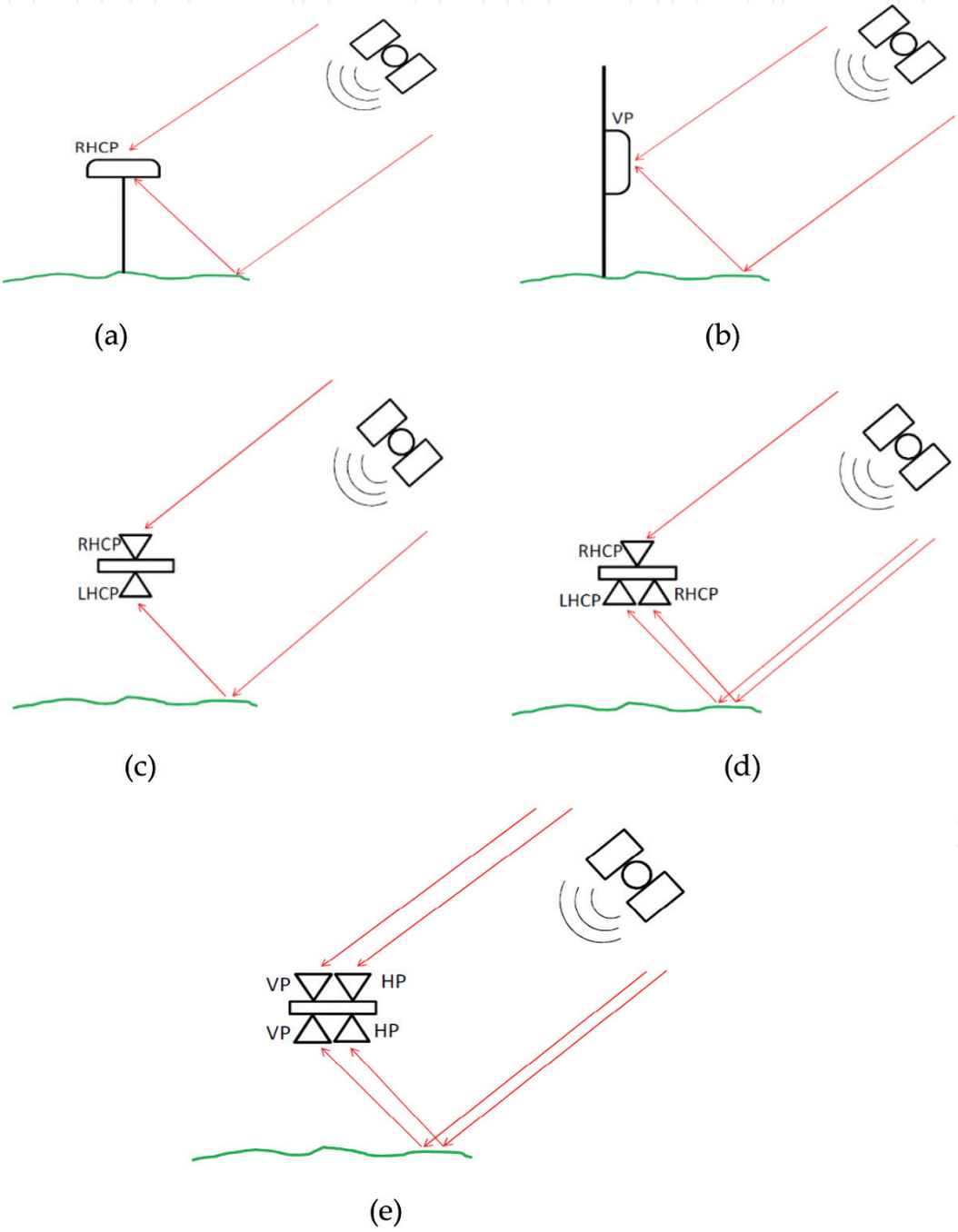

Figure 5. System schemes for different observing strategies.

of percentage of clay and sand should be known and provided in input to such models. A further model described by Topp et al. [39] does not depend on any input information, since it models the relative permittivity as a third-order polynomial function of soil moisture.

3.2.2. Bistatic methods for soil moisture retrieval

In this section, the algorithms used for SMC and vegetation sensing are applied based on the (5.a): bistatic method. The retrieval process aims to establish the link between received reflected signals and the dielectric constant of the soil. Moreover, the retrieval of dielectric constant is the key component to the retrieval of soil moisture, since there are several well-established models giving this relationship as introduced in the last section.

3.2.2.1. Only LH reflected GPS signals are measured

Assuming a perfectly smooth surface and regardless the surface roughness and incoherent components ($\Gamma_{lr} = (R_{lr}(\vartheta))^2$), the dielectric constant is retrieved from the LHCP-reflected SNR which can be processed by the open loop approach.

The expression of SNR is derived from bistatic radar equation:

$$SNR_{peak}^{reflect} = \frac{1}{4}\frac{P^t G^t}{4\pi(R_1+R_2)^2}\frac{G^r \lambda^2 G_D}{4\pi P_N}(R_{vv}-R_{hh})^2, \tag{13}$$

where P^t is transmitted signal power, G^t and G^r are antenna gains of transmitter and receiver, respectively. λ is signal wavelength (about 19 cm for GPS L1 signal). R_1 and R_2 represent the distances between specular point and transmitter or receiver. The superscript c denotes the coherent component, P_N is noise power, and G_D is the processing gain due to the de-spread of the GPS C/A code. The value of the correlation gain is determined by the chipping rate of the GPS L1 C/A code ($1.023e^6$ Hz) and 1 ms processing interval. It results:

$$G_{pr} = 10\log_{10}\left(\frac{1.023e^6}{1000}\right) = 30.1dB. \tag{14}$$

Fresnel reflection coefficients of *HH* and *VV* are given in Eqs. (7) and (8). The dielectric constant is then easy to be solved by combining the Eqs. (7), (8), and (13). Input parameters such as P^t, G^t, G^r, and G_D are usually seen to be constants. Since they are system parameters of GPS, P_N should be estimated or calculated properly. R_1, R_2, and θ are geographic information which can be calculated through receiver positions. SNR is the input parameter obtained from signal postprocessing. Knowing all the above input parameters, the dielectric constant can be solved numerically.

3.2.2.2. Both LH reflected and RH direct GPS signals are measured

In this case, both SNRs are obtained from RH direct signal and LH reflected signal. The dielectric constant can be retrieved from the power ratio of LHCP reflected SNR over direct

RHCP SNR, provided that direct RH signals are processed with the same open-loop approach to get SNR.

The SNR expression of the peak power for the direct RHCP signal is:

$$SNR_{peak}^{direct} = \frac{P^t G^t}{4\pi {R_3}^2} \frac{G^r \lambda^2 G_D}{4\pi P_N}, \tag{15}$$

where R_3 is the distance between the transmitter and receiver. It must be noted that receiver gain G^r and noise power P_N given in Eq. (15) are not equal to those given in Eq. (13) for the reflected signal path, and this is the reason why calibration is needed. By making the ratio of Eq. (13) to Eq. (15) canceling the same parameters and summarizing the uncertainties of G^r and P_N into a single calibration parameter C, we have:

$$\frac{SNR_{peak}^{reflect}}{SNR_{peak}^{direct}} = \frac{{R_3}^2}{4(R_1 + R_2)^2} (R_{vv} - R_{hh})^2 \cdot C. \tag{16}$$

Now, input parameters of R_1, R_2, θ and R_3 are only needed, and they are easy to obtain from positioning information. Calibration parameter C can be either ignored if there is no way to calibrate the system or calculated through over-water measurement. The dielectric constant can be obtained from Eq. (16), given all the input parameters defined.

3.2.2.3. Both LH reflected and RH reflected GPS signals are measured

The retrieval process has linked the measured reflected LHCP and RHCP power (or SNR) to the normalized bistatic radar cross section σ_{qp}^o, which has been widely studied and modeled for different surface roughness and scattering models, such as Kirchhoff Approximation in stationary-phase approximation (Kirchhoff Geometrical Optics, KGO), Kirchhoff approximation in physical optics approximation (KPO), and small perturbation method (SPM) [34].

Applying polarization scattering matrix [40] and combining some basic electromagnetic field theories, the cross-polarization power ratio of LHCP to RHCP has the relation with normalized bistatic radar cross section of linear polarizations:

$$\frac{\sqrt{P_{lr}^r}}{\sqrt{P_{rr}^r}} = \frac{\left|\sqrt{{\sigma^o}_{hh}} + \sqrt{{\sigma^o}_{vv}}\right|}{\left|\sqrt{{\sigma^o}_{hh}} - \sqrt{{\sigma^o}_{vv}}\right|}. \tag{17}$$

Note here that in Eq. (17), σ^o is approximated by the special case of $\sigma_{qp(spec)}^o$ in the specular direction for simplicity, and therefore, the cross polarization terms of ${\sigma^o}_{hv}$ and ${\sigma^o}_{vh}$ are computed to be zero for the models of KGO, KPO, and SPM in the specular direction case. Also, σ^o for *hh* and *vv* polarizations given by these three models are all products of a polarization sensitive parameter, usually the Fresnel reflection coefficient and other polarization independent surface roughness parameters (detailed expressions are given by [Ulaby, 1982]). Then, the expression shown in Eq. (17) can be simplified as:

$$\frac{\sqrt{P_{lr}{}^{r}}}{\sqrt{P_{rr}{}^{r}}} = \frac{||R_{hh}| + |R_{vv}||}{||R_{hh}| - |R_{vv}||}, \tag{18}$$

where R is the Fresnel reflection coefficient as given in Eqs. (7) and (8). This equation also holds the condition of specular reflection, and the result shows that the cross-polarization power ratio of LHCP to RHCP of reflected signals is independent with surface roughness and is only a function of dielectric constant and incident angle.

The received power for both *lr* and *rr* is obtained as input parameters after post-processing. The dielectric constant of the soil is solved after taking all the parameters.

3.2.3. Retrieval methods for vegetation biomass sensing

The GNSS signals in bistatic configuration were obtained by the cross-correlation between direct and reflected signals with the pseudo-random noise (PRN) code replica, respectively. The output of the cross-correlation is called Delay-Doppler map (DDM), and Delay Waveforms (DW) is a row from DDM with the Doppler frequency set to a constant value of where the peak is. The phase information of the signal is lost during the integration process, resulting in amplitude $< |Y_{pq}| >$ or power $< \left|Y_{pq}\right|^2 >$ waveforms for the incident q-polarized to p-polarized scattered signals. The observable polarimetric parameters Γ_{lr} and Γ_{rr} represent the cross and co-polar reflectivity can be defined as in [12]:

$$\Gamma_{pq} = \left| \left\langle \frac{Y^{peak}_{reflected,\, p(\Delta\tau, f)}}{Y^{peak}_{direct,\, q(0,f)}} \right\rangle \right|^2, \tag{19}$$

where $\Delta\tau$ is the delay difference between the direct and the reflected paths, and the f is assumed to be the Doppler frequency shift of the signal. With ground-based or low-altitude receivers, it also can be assumed to be the same, $f_d \approx f_r = f$. The above equation obtained both the coherent and incoherent component of the received direct and reflected signals. However, the unstable airborne platform, terrain variation, and fading phenomenon may impair the estimation of the coherent scattering component. By adding the time series, an averaging procedure can be used to remove the contribution of the incoherent component on the final observed reflectivity. It was written as:

$$\Gamma_{pq} = \left| < \frac{Y_{r,\, p(t)}}{Y_{d,\, q(t)}} > \right|^2 = < \left| \frac{Y_{r,\, p(t)}}{Y_{d,\, q(t)}} \right|^2 > - \delta^2_{\left| \frac{Y_{r,\, p(t)}}{Y_{d,\, q(t)}} \right|}. \tag{20}$$

After the reduction of the incoherent component from the received signal, the received signal is mainly composed of coherent components. Therefore, the spatial resolution can be roughly estimated from the first Fresnel zone [31]. For instance, the 600 m flight altitude and 40° incident angle lead to an elliptical active scattering area with a minor axis of 24 m and a major axis of 32 m. Finally, the reflectivities Γ_{lr} and Γ_{rr} and the ratio of Γ_{lr}/Γ_{rr}, which was called

polarimetric ratio (PR), are the three observable parameters used to investigate the SMC and the vegetation biomass of the terrain.

3.2.4. GPS C/A-code altimetry

The geometry of the reflecting surface with the receiver and transmitter is shown in **Figure 6** under the assumption of a flat Earth and ray optics. The path delay (δ) between the direct and the reflected signals can be taken as a delay difference ($N_{samples}$) in the DDM obtained from Eq. 21.

$$\delta = \frac{c}{f_s} N_{samples} = \frac{c}{f_s} \cdot \frac{N_{chip}}{1023/1ms} \cdot f_s, \tag{21}$$

where C is the light speed and f_s is the sampling frequency of the GNSS-reflectometer, and N_{chips} is the number of chips in one period.

Assuming that the signals are parallel as shown in **Figure 6**, it gives that $\theta = \alpha$ for the incoming signals. Height h is possible to be derived from the following equation [41, 42]:

$$h \approx \frac{\delta}{2 \sin \alpha}, \tag{22}$$

where δ is the excess path and θ is equal to the elevation angle α. Therefore, the estimated altitude of the receiver h depends on the measured delay between the two signals and the elevation of the satellite.

3.2.5. Data processing

The GNSS-R system used for the acquisition of the received power can measure both the direct GPS signal and the reflected one using two independent acquisition channels: one for the direct signal and the other for the reflected signal. The receiver consists of two commercial

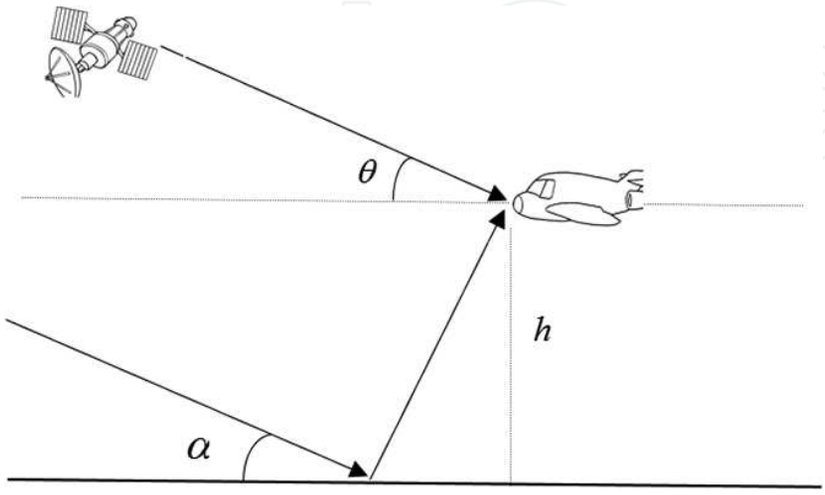

Figure 6. GNSS altimetry geometry with signals considered in a parallel condition.

front-ends (FEs) connected to two antennas: for instance, a traditional hemispherical GNSS L1 patch antenna pointed upward for the measurement of the direct signal. A high-gain LHCP antenna pointed downward for measuring the reflected signal as shown in **Figure 7**. Each FE is connected to a PC for data storage. The antennas and the FEs are mounted on a Kevlar bar. A typical tripod is used for more efficient adjustment of the orientation of the antennas.

The raw data of direct and reflected signals are collected and postprocessed with the software SOPRANO [43] for obtaining the peak power and SNR for each satellite. An open-loop approach is used for processing to obtain delay-Doppler maps (DDMs) and the corresponding delay waveforms. SNR time series were estimated from several noncoherently integrated delay waveforms generated by cross-correlation of the incoming data and local replica C/A codes.

Generally, increasing coherent integration time can help the low SNR to generate the DDM, but the performance may worsen when it exceeds a certain value. In this case, the coherent integration time was 1 ms because of the length of the GPS C/A code (1 ms). On the other hand, since the reflected signal power was attenuated by the surface as well as by the noise effects, it could not detect the real signal power. A noncoherent integration time technique (called averaging) was adopted during the postprocessing in order to mitigate the noise. Generally, it is in the range of 100-1000 ms. The noncoherent integration time, in this case is 500 ms. Moreover, the information of positions and altitude was recalculated, which was used to calculate the specular points on object areas. During the experiment, satellite positions (x, y, z) in an ECEF coordinate were collected by a GPS recorder. In the meanwhile, the receiver position (latitude, longitude, attitude) in geoid coordinate was collected in a file (.kml) which can be opened by the Google Earth software. The flowchart of obtaining the navigation message is shown in **Figure 8**.

The height coordinate z in the file (.kml) should be transferred into the WGS84 coordinate first, because the height z is in EGM96 coordinate system which already considered the sea surface altitude. The second step is to transfer the WGS84 coordinates (latitude, longitude, height) into the ECEF coordinate that can correlate with the satellite positions (x, y, z). With having receiver

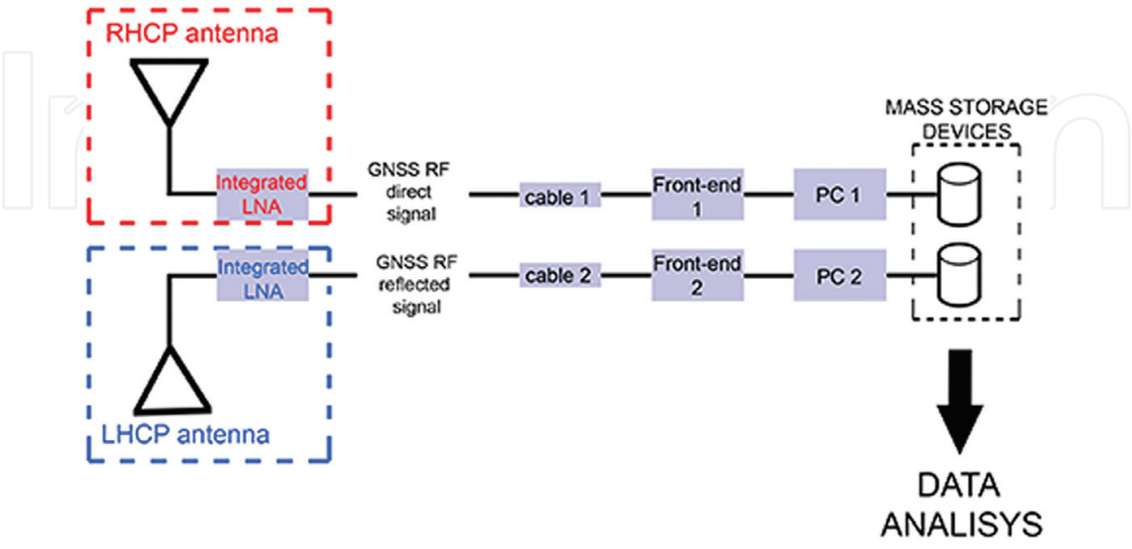

Figure 7. GNSS-R system block diagram: Antennas and front-end connections.

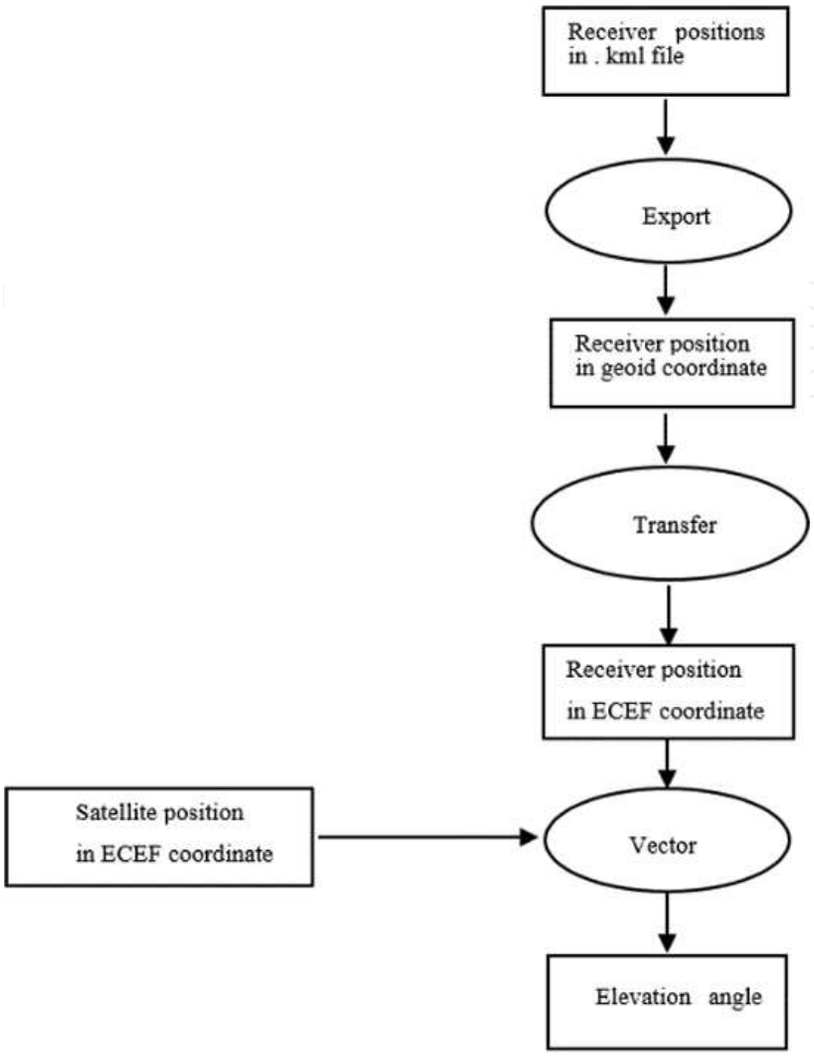

Figure 8. Flowchart of processing navigation message.

and satellite positions both in ECEF coordinates, elevation angle can be calculated with respect to the local tangent plane.

4. Results and discussions

A low-altitude airborne experiment was carried out by a P92 Digisky airplane over the Avigliana lake (45.099°N, 7.369°E) in Italy. An image of the experimental area from Google Map is shown in **Figure 9**.

In this area, there are two lakes, the size of the northern lake (bigger) is approximately 1 km x 1.3 km, while that of the southern lake (smaller) is 700 m × 1.1 km. The area was selected for the experiment because of the following reasons. First, the presence of two lakes of the experiment can provide the reflections and the known permittivity for calibration. Second, in the North and South directions of the two lakes, there are some grass areas which the flight

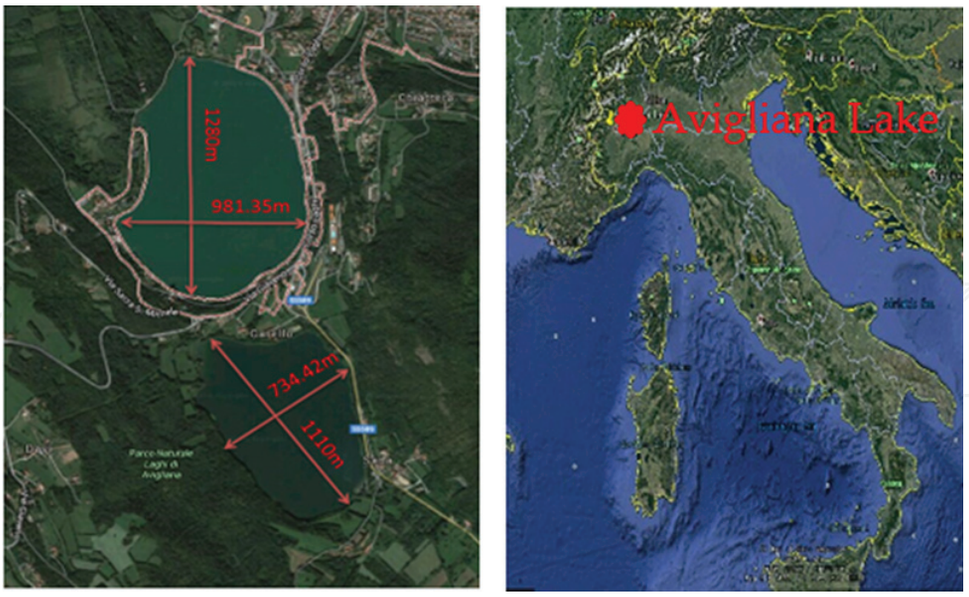

Figure 9. Avigliana area.

will go over, and in the West and East directions, the flight coverage areas are full of forest. This kind of geographical environment provides the possibility to investigate the roughness and vegetation biomass at the same time.

The elevation and azimuth angles were obtained, as shown in **Figure 8**. The sky plot of GPS satellites at the 1570th second of the flight is shown in **Figure 10**.

The reflected LHCP signal was collected through a high gain dual polarization antenna. With the direct RH signal obtained, the reflectivity was computed by the SNR of LH/RH signal

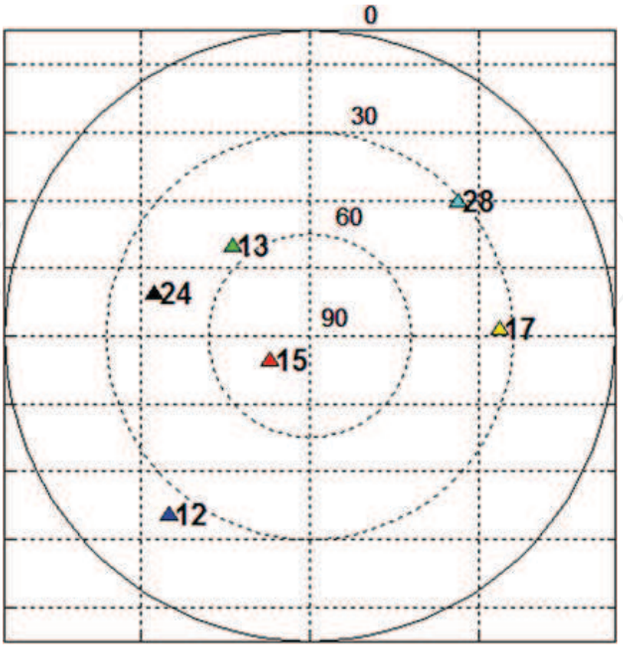

Figure 10. Sky plot of satellites on 18th June 2015.

component. The SMC was obtained by using the method introduced in Section 3.2.2. The SMC estimation result of PRN 15 with high elevation angle is shown in **Figure 11**, calibrated by the water reflectivity of 0.67. The color of the specular points is proportional to the estimated soil moisture (the red color denotes totally dry soil, and the green color represents humidity 100%).

The flight flew covered lake and two forest areas from east to west. The flight route was denoted by the yellow color in **Figure 12**. Since the reflection point begins from the forest in the east (mid-biomass) to big lake (flat) then stop with the forest in the west (big-biomass) as shown in **Figure 12**, it can be used to investigate the vegetation biomass sensing.

Based on the method introduced in Section 3.2.3, the reflectivities Γ_{lr} and Γ_{rr} and the ratio of the two polarization (*lr* and *rr*) PR can be calculated and shown in **Figure 13**. From 720 s, the big increment 6 dB of the average *lr* appears in the lake (L1) compared to the forest. The *lr* component is quite sensitive with SMC. The average *rr* in forests (F1 and F2) is 2–4 dB lower than the lake (L1). In addition, considering the average *lr* and *rr* in forests (F1 and F2), both

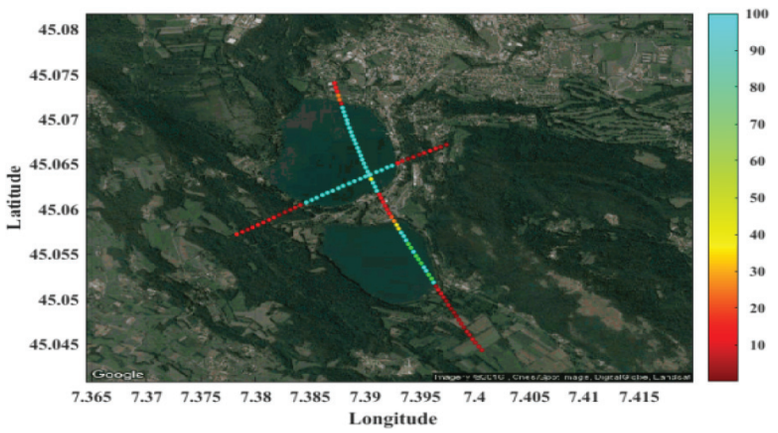

Figure 11. Soil moisture content estimation of PRN 15.

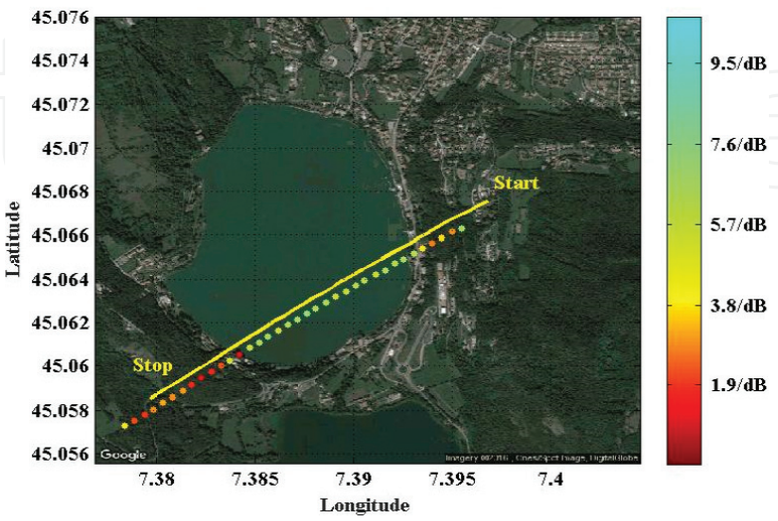

Figure 12. Flight route (yellow line) and PR level of reflection point georeferenced in Google Map.

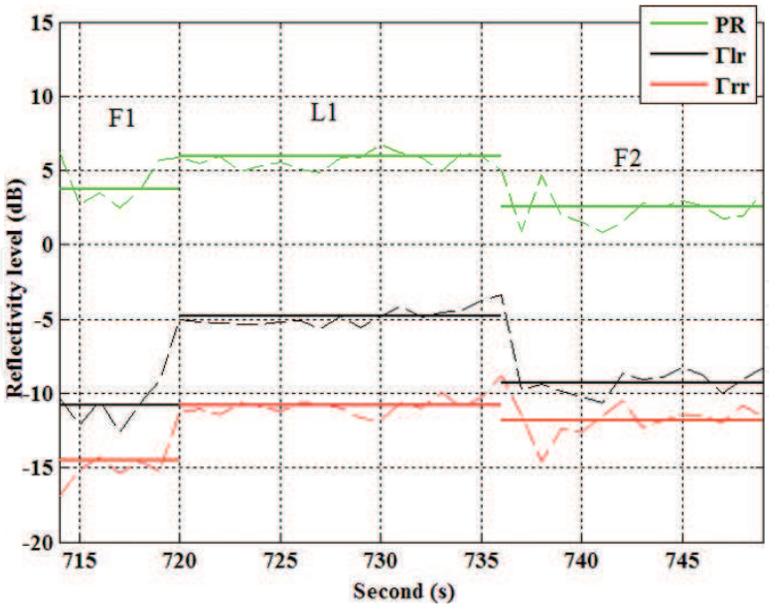

Figure 13. PR level, Γ_{lr} and Γ_{rr} level.

average in F2 are higher than F1. It could be considered that the vegetation biomass in F2 is lower than F1. It confirms the fact and further implies that both polarizations are sensitive to vegetation biomass. Moreover, the biggest PR level is the presence of the lake. Therefore, the PR can be taken as a good parameter for soil moisture estimation regardless of the vegetation biomass. The PR level is 5.6 dB in the lake, 3.9 dB in F1, and 2.3 in F2.

For the altimetry estimation, the C/A code method (see Section 3.2.4) was applied on the unsmooth surface to obtain the target height. Due to bandwidth and the equipment, the altimetry

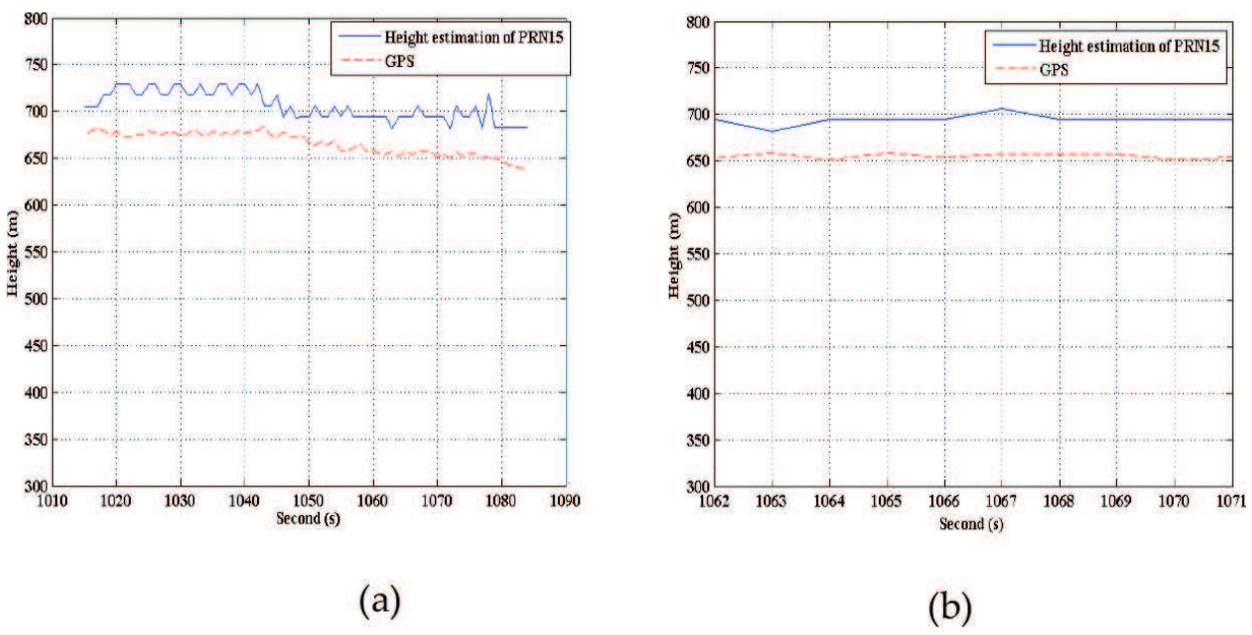

Figure 14. Altimetry estimation of PRN 15 from 1015s (a), 1062s (b).

resolution is limited, according to 1 sample 23.07 m. The altimetry estimation results of satellite PRN 15 with high elevation angle are presented in **Figure 14**.

Figure 14 shows two figures of height estimation of PRN 15 start from 1015s and 1062s. The elevation angle of PRN 15 is 76°. The estimation height is quite same with GPS recorder. The estimation deviation in **Figure 14 (a)** is bigger than **Figure 14 (b)**. It confirmed that the best condition for altimetry application is when using high elevation angle on the water surface, which can greatly avoid the interference of forest and cities. The accuracy of the altimetry estimation depends on the bandwidth, algorithm, and equipment, and it shows that it is quite affected by the environment as introduced in the beginning of Section 3.

5. Conclusion

In this chapter, the global navigation satellite system-reflectometry (GNSS-R) technique as a method of remote sensing that receives and processes microwave signals reflected from various surfaces to extract useful information is reported. GNSS-R technique has gained widespread attention in a variety of applications. This work assesses the capability of measuring soil moisture and vegetation biomass by means of reflected signals from global navigation satellites from a theoretical and experimental point of view.

The SMC was obtained and georeferenced in Google Maps. The type of terrain ranged from water (on the lakes) to terrain with small bushes to built-up areas. The results showed good correlation with the types of the underlying terrain. It was observed that the LH was rather more sensitive to SMC. The different SMC areas were detected with different PR values. The ratio of the two polarizations was independent of roughness, and it proved to be an optimum parameter for soil moisture estimation. Moreover, it was found that increasing the biomass quantity decreased the Γ_{lr} and Γ_{lr} polarization components, since the reflected signal components are attenuated from leaves, trunks, crowns, and so on. The altimetry estimation is based on the calculation of the delay differences between the two signals. In principle, the altimetry techniques can be applied to any surface, but their performance will depend on the scattering behavior. Therefore, GNSS-R altimetry has only been used on strongly reflecting surfaces and geometries, such as waters and smooth ice. The accuracy of the derived height is limited also due to the bandwidth and the sampling frequency of the equipment.

Acknowledgements

Some of the works illustrated in this chapter were developed by the authors and their collaborators at the University of Politecnico di Torino. The authors would like to thank the SMAT-F2 project, ISMB and all the researchers involved. Furthermore, this research is financed by National Science Foundation of China under projects No. 61601076 and sponsored by NUPTSF (Grant No. 217152).

Author details

Yan Jia[1] and Yuekun Pei[2]*

*Address all correspondence to: peiyuekun@dlu.edu.cn

1 Nanjing University of Posts and Telecommunications, Nanjing, China

2 Dalian University, Dalian, China

References

[1] Jin S, Feng G, Gleason S. Remote sensing using GNSS signals: Current status and future directions. Advances in Space Research. 2011;**47**(10)

[2] Dawoud S. GNSS Principles and Comparison. Potsdam: Potsdam University; n.d

[3] Groves P. Principles of GNSS, Inertial, and Multisensor Integrated Navigation Systems. London: Artech house; 2013

[4] Hofmann-Wellenhof B, Lichtenegger H, Wasle E. GNSS–Global Navigation Satellite Systems: GPS, GLONASS, Galileo, and More. New York: Springer Science & Business Media; 2007

[5] Parkinson B. Progress in Astronautics and Aeronautics: Global Positioning System: Theory and Applications. Reston: Aiaa; 1996

[6] Betz J. Signal structures for satellite-based navigation: Past, present, and future. Inside GNSS. 2013;**8**:34-42

[7] Zavorotny V, Voronovich A. Scattering of GPS signals from the ocean with wind remote sensing application. IEEE Transactions on Geoscience and Remote Sensing. 2000;**38**(2): 951-964

[8] Cardellach E, Fabra F, Nogués-Correig O, Oliveras S, Ribó S, Rius A. GNSS-R ground-based and airborne campaigns for ocean, land, ice, and snow techniques: Application to the GOLD-RTR data sets. Radio Science. 2011;**46**(6):1-16

[9] Larson K, Braun J, Small E, Zavorotny V, Gutmann E, Bilich A. GPS multipath and its relation to near- surface soil moisture content. IEEE Journal of Selected Topics in Applied Earth Observation and Remote Sensing. 2010;**3**(1):91-99

[10] Jia Y, Savi P. Sensing soil moisture and vegetation using GNSS-R polarimetric measurement. Advances in Space Research. 2017:858-869

[11] Jia Y, Savi P, Canone D, Notarpietro R. Estimation of surface characteristics using GNSS LH-reflected signals: Land versus water. IEEE Journal of Selected Topics in Applied Earth Observations and Remote Sensing. 2016;**9**(10):4752-4758

[12] Egido A, Caparrini M, Ruffini G, Paloscia S, Santi E, Guerriero L, et al. Global navigation satellite systems reflectometry as a remote sensing tool for agriculture. Remote Sensor. 2012;**4**(8):2356-2372

[13] Hugo C, Amèzaga A, Vidal D, Olivé R, Munoz J, Camps A. First polarimetric GNSS-R measurements from a stratospheric flight over boreal forests. Remote Sensing. 2015;**7**(10): 13120-13138

[14] Beckmann P, Spizzichino A. The Scattering of Electromagnetic Waves from Rough Surfaces. New York, USA: Artech House; 1987

[15] Katzberg S, Garrison J Jr. Utilizing GPS to determine ionospheric delay over the ocean. NASA T. R. TM-4750; 1996

[16] Willis NJ. Bistatic Radar, British Library. London: British Library; 1995

[17] Martin-Neira M. A passive reflectometry and interferometry system (PARIS): Application to ocean altimetry. ESA Journal. 1993;**17**:331-355

[18] De Roo R, Ulaby F. Bistatic specular scattering from rough dielectric surfaces. IEEE Transactions on Antennas and Propagation. 1994;**42**(2):220-231

[19] Stutzman W. Polarization in Electromagnetic Systems. London: Artech house; 1993

[20] Misra P, Enge P. Global Positioning System: Signals, Measurements and Performance. Lincoln, MA: Ganga-Jamuna Press; 2006

[21] Lemoine F, Kenyon S, Factor J, Trimmer R, Pavlis N, Chinn D, … Wang Y, Lemoine, Frank G, et al. The Development of the Joint NASA GSFC and the National Imagery and Mapping Agency (NIMA) Geopotential Model EGM96. NASA/TP-1998-206861; 1998

[22] Rodriguez-Alvarez N, Camps A, Vall-Llossera M, Bosch-Lluis X, Monerris A, Ramos-Perez I, et al. Land geophysical parameters retrieval using the interference pattern GNSS-R technique. IEEE Transactions on Geoscience and Remote Sensing. 2011;**49**(1):71-84

[23] Ruffini N, Soulat F, Caparrini M, Germain O, Martín-Neira M. The Eddy experiment: Accurate GNSS-R ocean altimetry from low altitude aircraft. Geophysical Research Letters. 2004;**31**(12):L12306

[24] Rius A, Cardellach E, Martin-Neira M. Altimetric analysis of the sea-surface GPS-reflected signals. IEEE Transactions on Geoscience and Remote Sensing. 2010;**48**(4–2):2119-2127

[25] Wang J, Schmugge T. An empirical model for the complex dielectric permittivity of soils as a function of water content. IEEE Transactions on Geoscience and Remote Sensing. 1980;**4**:288-295

[26] Njoku E, O'Neill P. Multifrequency microwave radiometer measurements of soil moisture. IEEE Transactions on Geoscience and Remote Sensing. 1982;**4**:468-475

[27] Zavorotny V, Larson K, Braun J, Small E, Gutmann E, Bilich A. A physical model for GPS multipath caused by land reflections: Towards bare soil moisture retrieval. IEEE Journal of Selected Topics in Applied Earth Observation and Remote Sensing. 2010;**3**(1):100-110

[28] Mironov V, Kosolapova L, Fomin S. Physically and mineralogically based spectroscopic dielectric model for moist soils. IEEE Transactions on Geoscience and Remote Sensing. 2009:2059-2070

[29] Mironov V, Muzalevskiy K. The new algorithm for retrieval of soil moisture and surface roughness from GNSS reflectometry. In: IEEE International Geoscience and Remote Sensing Symposium. Munich: IEEE; 2012. pp. 7530-7532

[30] Rodriguez-Alvarez N, Bosch-Lluis X, Camps A, Vall-Llossera M, Valencia E, Marchan-Hernandez J, Ramos-Perez I. Soil moisture retrieval using GNSS-R techniques: Experimental results over a bare soil field. IEEE Transactions on Geoscience and Remote Sensing. 2009; **47**(11):3616-3624

[31] Masters D, Axelrad P, Katzberg S. Initial results of land-reflected GPS bistatic radar measurements in SMEX02. Remote Sensing of Environment. 2004;**92**(4):507-520

[32] Gleason S, Hodgart S, Sun Y, Gommenginger C, Mackin S, Adjrad M, Unwin M. Detection and processing of bistatically reflected GPS signals from low earth orbit for the purpose of ocean remote sensing. IEEE Transactions on Geoscience and Remote Sensing. 2005;**43**(6):1229-1241

[33] Katzberg S, Torres O, Grant M, Masters D. Utilizing calibrated GPS reflected signals to estimate soil reflectivity and dielectric constant: Results from SMEX02. Remote Sensing of Environment. 2006;**100**(1):17-28

[34] Ulaby F, Moore R, Fung A. Microwave Remote Sensing Active and Passive-Volume II: Radar Remote Sensing and Surface Scattering and Enission Theory. New York, USA: Artech House; 1982

[35] Pierdicca N, Guerriero L, Giusto R, Brogioni M, Egido A, Floury N. GNSS reflections from bare and vegetated soils: Experimental validation of an end-to-end simulator. In: 2011 IEEE International Geoscience and Remote Sensing Symposium (IGARSS). Vancouver, BC, Canada: IEEE; 2011. pp. 4371-4374

[36] Ceraldi E, Franceschetti G, Iodice A, Riccio D, Ruello G. On the use of the specular direction copolarised ratio for the retrieval of soil dielectric constant. In: 2003 IEEE Geoscience and Remote Sensing Symposium. Vol. 7. Toulouse, France: IEEE; 2003. pp. 4144-4146

[37] Hallikainen M, Ulaby F, Dobson M, El-Rayes M, Wu L. Microwave dielectric behavior of wet soil-part 1: Empirical models and experimental observations. IEEE Transactions on Geoscience and Remote Sensing. 1985;**1**:25-34

[38] Dobson M, Ulaby F, Hallikainen M, El-Rayes M. Microwave dielectric behavior of wet soil—Part II: Dielectric mixing models. IEEE Transactions on Geoscience and Remote Sensing. 1985;**23**(1):35-46

[39] Topp G, Davis J, Annan A. Electromagnetic determination of soil water content: Measurements in coaxial transmission lines. Water Resources Research. 1980;**16**(3):574-582

[40] Knott E. Radar Cross Section Measurements. New York, U.S.A.: Springer Science & Business Media; 2012

[41] Martín-Neira M, Caparrini M, Font-Rosselló J, Lannelongue S, Vallmitjana C. The PARIS concept: An experimental demonstration of sea surface altimetry using GPS reflected signals. Remote Sensing. 2001;**39**:142-149

[42] Helm A. Ground-Based GPS Altimetry with the L1 OpenGPS Receiver Using Carrier Phase Delay Observations of Reflected GPS Signals. GFZ German Research Centre for Geosciences; 2008 Available: www.gfz-potsdam.de

[43] Falletti E, Margaria D, Nicola M, Povero G, Troglia Gamba M. N-FUELS and SOPRANO: Educational tools for simulation, analysis and processing of satellite navigation signals. In: IEEE International Conference on Frontiers in Education. Oklahoma, USA: IEEE; 2013. pp. 303-308